Cortical depth-dependent human fMRI of resting-state networks using EPIK

Authors

Patricia Pais-Roldán[1], Seong Dae Yun[1], Nicola Palomero-Gallagher[2-4], N. Jon Shah[1,5-7*]

[1]Institute of Neuroscience and Medicine 4, Medical Imaging Physics, Forschungszentrum Jülich, Germany

[2]Institute of Neuroscience and Medicine 1, Structural and Functional Organisation of the Brain, Forschungszentrum Jülich, Germany

[3]C. & O. Vogt Institute for Brain Research, Heinrich-Heine-University, 40225 Düsseldorf, Germany

[4]Department of Psychiatry, Psychotherapy and Psychosomatics, Medical Faculty, RWTH Aachen, Aachen, Germany

[5]Institute of Neuroscience and Medicine 11, Molecular Neuroscience and Neuroimaging, JARA, Forschungszentrum Jülich, Germany

[6]JARA - BRAIN - Translational Medicine, Aachen, Germany

[7]Department of Neurology, RWTH Aachen University, Aachen, Germany

ORCIDs

Patricia Pais-Roldán (https://orcid.org/0000-0002-9381-3048)

Seong Dae Yun (https://orcid.org/0000-0001-7398-1899)

Nicola Palomero-Gallagher (https://orcid.org/0000-0003-4463-8578)

N. Jon Shah (https://orcid.org/0000-0002-8151-6169)

E-mail

Patricia Pais-Roldán (p.pais@fz-juelich.de)

Seong Dae Yun (s.yun@fz-juelich.de)

Nicola Palomero-Gallagher (n.palomero-gallagher@fz-juelich.de)

N. Jon Shah* (n.j.shah@fz-juelich.de)

Keywords

Cerebral cortex, Cortical Layer, Resting-state fMRI, High-resolution, EPIK

Author Contributions

N.J.S. designed the research; S.Y. developed the MR imaging sequence and the corresponding image reconstruction software; S.Y. and P.P. performed in vivo experiments. P.P. designed and performed all data analysis; P.P. wrote the manuscript and prepared all figures; N.J.S. invented the original EPIK sequence; N.P.-G. verified the anatomical labels and wrote the cytoarchitecture-related discussions; S.Y., N.P.-G. and N.J.S. reviewed the manuscript.

ABSTRACT

Recent laminar-fMRI studies have provided substantial understanding of the evoked cortical responses in multiple sub-systems; in contrast, the laminar component of resting-state networks remains largely unknown. Here, we used EPIK, which offers unprecedented coverage at sub-millimetre resolution, to investigate cortical resting-state dynamics with depth specificity. After verifying laminar activation profiles in response to a task, we investigated whole-brain laminar dynamics. During rest, signal oscillations were stronger in the superficial layers of the cortical ribbon, and functional connectivity analysis indicated that most resting-state cortical connections occurring at rest involve supra-granular layers. Coherence assessed in a lateral motor network suggested a modified distribution of layer-specific responses during task performance compared to resting-state. Whole-brain evaluation of laminar-fMRI encompasses unprecedented computational challenges; nonetheless, it enables a new dimension of the human cerebral cortex to be investigated from a global view, which may be key in the characterization of neurological disorders from a novel perspective.

Significance statement

Resting-state networks sustain conscious awareness and diverse cognitive processing in the absence of tasks. In contrast to cortical *areas*, the cortical *depth*-specific signals across different networks have been poorly investigated, mainly due to the small brain coverage enforced in high-resolution imaging methods. Here, we demonstrate the different involvement of the cortical layers in the maintenance of the resting-state dynamics at near whole-brain level, using an optimized fMRI sequence. Given the cytoarchitectonics of the human neocortex, and based on our results, the cortical thickness constitutes an important dimension to characterize the resting-state oscillations in the healthy brain and its functional study may facilitate the identification of novel targets in neurological diseases.

INTRODUCTION

In the mammalian brain, the cerebral cortex is organized into specialized functional areas across its surface. In humans, the largest part of the cerebral cortex is occupied by neocortex, where the perikarya of multiple neuronal cell types are organized into six horizontal layers. The layered structure of the neocortex, which can be characterized by its cytoarchitecture, is involved in specialized signal processing [1-3]. The functional specificity of the cortex at its different depths has been demonstrated in animals using multi-site electrodes and, more recently, with cell-specific calcium imaging, e.g., via two-photon microscopy or optical fibers [4-8]. Although electrophysiology can theoretically be performed in the human brain to investigate layer-specific activations, it is an extremely invasive technique and, consequently, data are only available from select patient groups, e.g., in epileptic patients, who benefit from such an undertaking [9]. Moreover, although electrode recordings can provide direct information concerning layer activity, the coverage of most electrophysiological recordings is limited by the number of multi-site electrodes which is usually a single point at different depths. Hence, due to a lack of non-invasive methods to sufficiently sample the cerebral cortex, the specific way in which the cortical neurons communicate with each other in the human brain -across different depths and through different areas- largely remains an open challenge.

In contrast to the limitations of electrophysiology, functional magnetic resonance imaging (fMRI) is a non-invasive technique with broad brain coverage capabilities. fMRI most commonly relies on the identification of blood changes, which, assuming perfect neuro-vascular coupling, represent neuronal function in the brain [10-12]. Despite its dependence on the vascular architecture of the cortex, laminar fMRI, i.e., sub-millimeter resolution fMRI acquired with the purpose of studying depth-specific neuronal responses, has proven to be a valuable tool for studying cortical dynamics in animals and humans [13-23]. Two main fMRI contrasts are usually employed in human laminar fMRI: cerebral blood volume (CBV), typically applied as part of vascular occupancy schemes (VASO), and blood oxygenation level dependent (BOLD). Although VASO offers high spatial specificity by detecting dilation of the microvasculature based on T1 contrast, it exhibits low sensitivity due to unwanted tissue suppression by an inversion recovery pulse [24-26]. In contrast, sequences based on BOLD present the advantage of a higher signal-to-noise ratio (SNR), with spin-echo-based (SE) echo planar imaging sequences (EPI) offering greater parenchymal specificity and gradient-echo (GE) schemes offering the best sensitivity [27]. The higher SNR and the flexibility to be able to accommodate higher sampling rates makes GE sequences some of the most commonly used in the fMRI field, typically in the form of GE-EPI. Due to GE schemes having enhanced sensitivity to large vessels [28], e.g., pial veins, with long T2* constants, several methods have been presented for use in the pre-processing pipeline to ameliorate contamination from extra-parenchymal signals or to correct the evoked activation profile across cortical depths [29-35].

fMRI acquired with different contrasts and sub-millimeter resolution has enabled the function of the cerebral cortex to be sampled with column- and layer-specificity in the context of sensory, motor, visual and auditory tasks [13, 15-23, 36-38], and has shown the superficial layers of the neocortex to be predominantly involved in the processing of neuronal signals. This predominance is possibly due to fact that layer III is the main source

and target of cortico-cortical connectivity [39], coupled with the higher synaptic density found there compared to the remaining cortical layers, and which is associated with higher receptor densities [1]. Importantly, a study focusing on the visual cortex reported correlations between the function of specific layers imaged with fMRI and particular EEG rhythms [40], reinforcing the potential for using fMRI to detect layer variability.

In contrast to task-related circuits, which are usually limited to specialized responses in a small portion of the cerebral cortex, during rest, cross-talk between distant cortical areas maintains a baseline neurological state [41]. Although the potential for using fMRI to sample cortical layers is clear, the limited brain coverage enforced by most existing high-resolution-fMRI schemes precludes the investigation of large-scale inter-regional depth-dependent connections. To date, only a few groups have reported fMRI acquisitions from the whole brain at ≤ 1 mm resolution [42-44] and, to our knowledge, only one study has intended to use laminar fMRI to uncover the cross-layer functional interactions that exist in the human brain during rest with a nominal spatial resolution of $0.8 \times 0.8 \times 0.8$ mm^3 [44].

Here, we applied TR-external EPIK, to identify the laminar signals from most of the cerebral cortex with a 0.63 mm iso-voxel size in healthy volunteers. It has been previously shown that EPIK [45-50] can offer higher spatial resolution in dynamic MR studies with comparable hemodynamic-response detection compared to routine EPI [51-55]. Moreover, the combination of TR-external phase correction with EPIK has been shown to offer a further enhancement of the spatial resolution [49, 56]. In this work, TR-external EPIK was optimized to almost entirely cover the human brain with 123 slices sampling voxel volumes of ~ 0.25 mm^3, estimated to enclose ~ 17500 neurons; for reference purposes, a 1 mm^3 voxel would enclose ~ 70000 neurons. The combination of smaller voxel size and near whole-brain coverage is a key feature of this work when compared to previous laminar fMRI studies. By adding pre-processing steps to correct for the potential bias of the GE sequence, e.g., using the phase component of the MR signal as a regressor, the acquired images allowed us to perform cortical depth dependent analysis of broad resting-state networking in the human brain.

RESULTS

1. Characterization of the cortical template for whole-brain laminar mapping

In a recent report, we have demonstrated the feasibility of using TR-external EPIK to assess fMRI activity over a large FOV with submillimeter spatial resolution [49]. The additional acquisition of a structural MP2RAGE sequence enabled us to produce a surface model of the cerebral cortex for each subject. Based on this model, it was possible to study brain activity at six different cortical depths, referred to hereafter as "layers" (different from the cytoarchitectonically-defined cortical layers) and specified as "white, +20%, +40%, +60%, +80% and pial", from the deepest to most superficial, respectively. These layers were used as a template for analysis of the functional data (see *Methods* and **Fig. 1**).

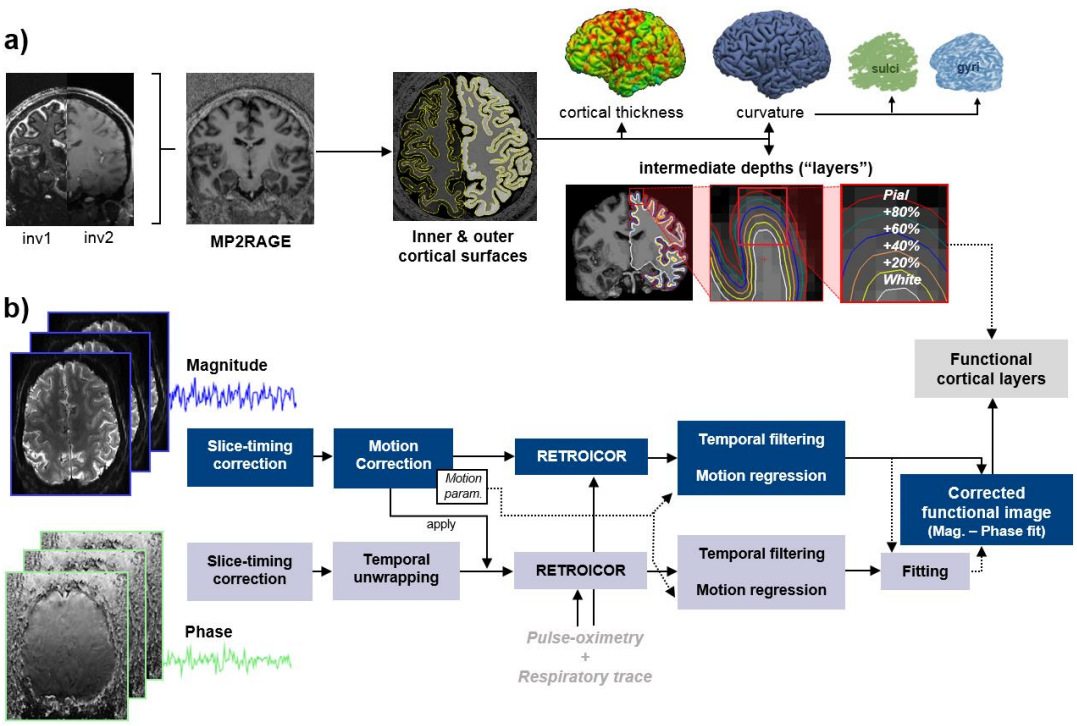

Figure 1. Main steps for pre-processing of the anatomical (a) and functional scans (b). a) *"inv1" and "inv2" indicate the first and second inversion contrast images of MP2RAGE. The T1-weighted MP2RAGE is used to segment the brain into gray matter, white matter, and CSF. The cerebral cortex (outer brain gray matter) is further processed to extract its boundaries (outer or "pial" and inner or "white"). Several calculations can be performed based on these surfaces (e.g., thickness, curvature). Four additional surfaces are generated at equal spacing.* ***b)*** *Both the magnitude and phase images obtained with TR-external EPIK are subjected to a routine pre-processing pipeline including slice timing correction, motion correction, regression of physiological signals and temporal filtering. The pre-processed phase image is used to correct the magnitude image from vein-related bias. The corrected pre-processed magnitude functional image is then projected onto the six generated surfaces, in subject space, for laminar fMRI analysis.*

Figure 2 provides a characterization of the cortical model. In **Figure 2a**, an example of the distribution of sulci and gyri, i.e., the curvature of the cerebral cortex, and cortical thickness is provided on a representative coronal slice. The spatial resolution of each surface was assessed in sulci and gyri independently. As the cortical surfaces were generated by inflating the inner cortical boundary towards the pial space, a one-to-one correspondence between vertices existed across all surfaces; hence, the in-surface resolution varied depending on the depth and the curvature (for a visual example, see insets in **Fig. 2b**). The histograms in **Figure 2b** show the distribution of vertex-to-vertex distances at different cortical depths for gyri (blue) and sulci (green), in both cerebral hemispheres, as a mean ± standard deviation (SD), obtained from an 18-subject group. In agreement with previous work [28], it could be observed that, in gyri, the vertex-to-vertex distance increased from 'white' to 'pial'; on average, a sparse distance of 0.72±0.04 mm existed between the vertices in the pial surface, whereas this distance was 0.49±0.01 mm in the white surface, i.e., the surface spatial resolution improved with depth in gyri locations. In contrast, in sulci, the vertex-to-vertex distance decreased from 'white'

to 'pial', with an average of 0.36±0.01 mm between consecutive vertices in the pial surface vs. 0.49±0.02 mm between the vertices of the deepest layer, i.e., outer surfaces were more densely sampled in sulci. This feature was observed in both the left and right hemispheres. The upper inset in **Figure 2b** exemplifies the larger vertex-to-vertex distance in the superficial layers of the cortical gyri, and the inset below exemplifies the larger distance between consecutive vertices in gyri compared to sulci. Cortical thickness was calculated in both cerebral hemispheres for 21 ROIs and for gyri and sulci in the whole cortex (**Fig. 2c**). Note that the analysis specific to gyri or sulci only considered the bottom 20% and top 20% curvature values, respectively (see *Methods*). Given that the cortical ribbon is thicker in the crown of gyri than in their walls or in the fundus of sulci [57] (**Fig. 2c**, blue bar vs. green bar), the layer-to-layer separation is greater at this position of the gyri (**Fig. 2d**, 0.62±0.02 mm between layers of cortical gyri vs. 0.40±0.01 mm in sulcal locations), which indicates that a higher signal contamination from neighboring layers can be expected in sulci, particularly in their fundus. Note that the in-depth resolution in the crown of gyri, i.e., the inter-layer distance, approximately corresponds to the voxel size employed in our fMRI protocol. Overall, across 18 subjects these robust cortical features were observed to be in agreement with the literature [28]. This suggests that the chosen subject-specific cortical model could be used as a reliable template to map functional signals and to study layer-based functional oscillations.

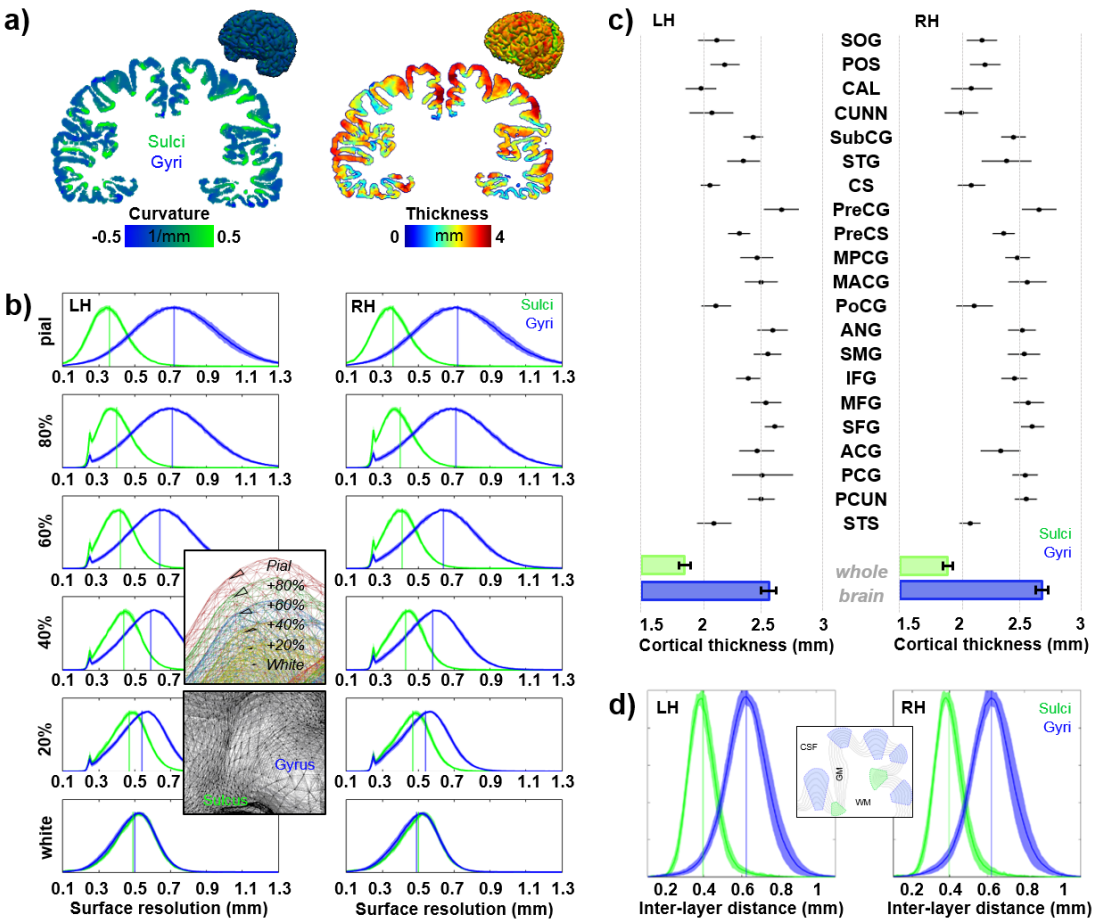

Figure 2. Evaluation of the cortical model. a) *Coronal slices showing the curvature and thickness of the cerebral cortex in a representative subject.* ***b)*** *Histograms showing the distribution of distances between two consecutive vertices at six different cortical depths, for locations corresponding to gyri (blue traces) or sulci*

(green traces), in both cerebral hemispheres. The insets show an example of the cortical surfaces in a gyrus (upper inset –an individual triangle is highlighted on each surface-) and of the pial surface over a sulcus and a gyrus (lower inset). ***c)*** *Cortical thickness calculated in 21 ROIs and mean cortical thickness calculated from the whole brain in gyri and sulci, for both cerebral hemispheres (mean ±SD, N=18).* ***d)*** *Histograms showing the distribution of the distance between vertices located in contiguous layers (e.g., white–layer02, layer02-layer04; etc.), for gyri and sulci, in both cerebral hemispheres. Histogram plots show normalized mean ± SD (N=18).*

2. Depth-dependent evoked responses in the primary motor cortex (M1)

In order to prove the capabilities of TR-external EPIK for use in a laminar analysis of the whole brain, we first aimed to reproduce the results obtained in previous fMRI studies of finger-motor tasks. These results are characterized by a strong response in the upper layers of M1 and a second activation peak in the middle-deep layers when avoiding non-corrected GE-BOLD sequences [16-18]. A task-based fMRI protocol consisting of 12 epochs, alternating 21 s blocks of finger motion with 21 s blocks of rest, was conducted on each volunteer using a submillimeter-resolution protocol configured with TR-external EPIK; voxel size: 0.63 mm isotropic, matrix: 336 × 336, 123 slices (see protocol-1 in *Methods*). In agreement with the previous literature [16-18], we observed a marked predominance of the BOLD response in the superficial layers of M1 (**Fig. 3**). A monotonous signal decrease from superficial to deep layers, typical in GE-BOLD, was observed after averaging the beta coefficient within a portion of M1 (**Fig. 3c**, N=17), possibly partially reflecting a bias towards large venous vessels located on the surface (**Fig. S1**). However, when sampling the beta-map using only a few lines within area M1-4A [58], we were able to identify a bimodal response (**Fig. 3i-k**) typical of finger motor tasks finely assessed with line profiling in high-resolution schemes [16-18]. The specificity of laminar responses was further evaluated by comparing the activation profiles of two different tasks: movement-only, or movement + touch, i.e., somatomotion, or movement + somatosensation. While both tasks resulted in an initial activation peak in the superficial layers, the relatively salient response observed in deeper layers during movement was minimized and shifted towards more superficial layers upon addition of touch (**Fig. 3l**). Following a series of post-hoc correction steps to ameliorate the GE-BOLD signal bias towards pial vessels (see *Methods* and **Fig. S2**) [29, 30], the results obtained from the task-fMRI scans suggested that the submillimeter-resolution protocol obtained with TR-external EPIK is a reliable method for investigating whole-brain function with cortical depth specificity.

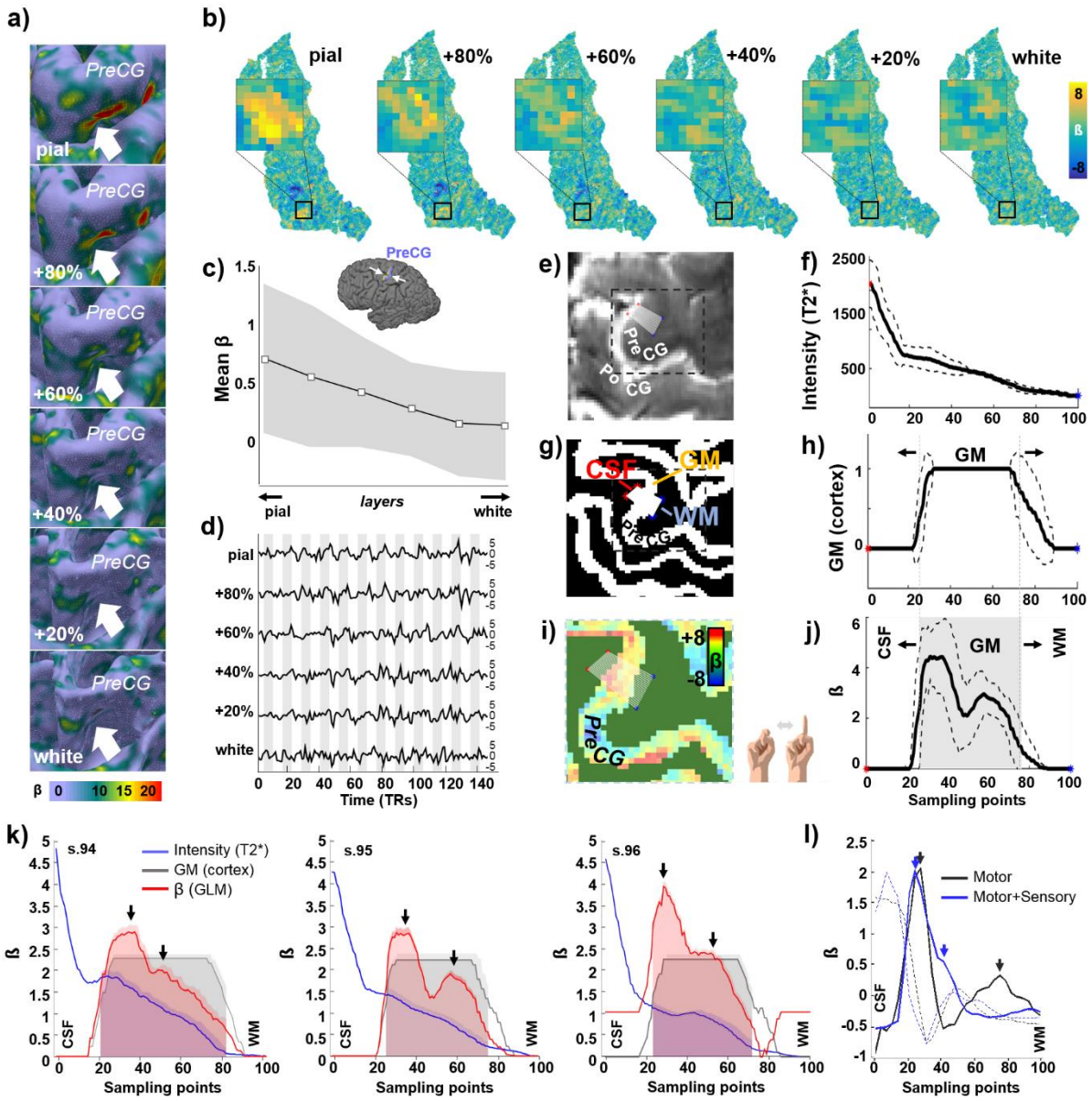

Figure 3. Cortical depth dependent motor task-evoked BOLD fMRI. a) *Six panels showing the surface beta-map for a finger motor task in six different cortical layers from a representative subject (a white arrow points to the main activated area of the PreCG).* ***b)*** *Representative flattened patches of the left PreCG extracted from six surfaces at different cortical depths. The inset over each patch is a magnified view displaying the best response, which was used for quantitative analysis of the surface-based GLM results.* ***c)*** *The graph shows the mean ±SD of the beta-coefficient in six different cortical layers, from the pial surface of the brain towards the inner white matter boundary (N=18).* ***d)*** *BOLD signal time courses extracted from a PreCG vertex at six different cortical depths.* ***e)*** *The figure shows part of a mean EPIK axial slice containing the PreCG. The twenty overlaid sampling lines (in white) extend from the CSF, covering the cortical thickness, up to the white matter (WM).* ***f)*** *Average line profile of the mean EPIK on the selected sampling region (the 20 lines on e)). Note the high intensity at the initial points (CSF, with long T2 constant) and the lower intensity at the intermediate points (cortical gray matter with the influence of veins, short T2). The discontinued lines represent the mean ±SD.* ***g)*** *Same region as in e), cropped from the segmented MP2RAGE, which identifies the cortical ribbon (in*

white color, labeled as gray matter (GM)). ***h)*** *Line profile calculated from the sampling lines over the image in g).* ***i)*** *Beta coefficient map overlaid on the segmented MP2RAGE.* ***j)*** *Profile of the beta coefficient along the selected lines crossing the finger area in the PreCG. Note the higher signal on upper and middle layers of the cerebral cortex (double peak, typical of motor tasks).* ***k)*** *Three examples showing the line profiles of the beta map in three consecutive slices (s94.s96). The black arrows highlight the most salient signals across the cortical ribbon. The gray-shaded area in j) and k) represents the extent of the gray matter, with superficial layers (i.e., pial surface) on the left, near the CSF, and deep layers (i.e., white surface), on the right, near the white matter.* ***l)*** *Line profiles in a different volunteer performing either a finger movement (black trace) or a finger movement plus touch (blue trace). Dashed lines indicate the intensity of the mean functional image for each task-fMRI scan, for localization purposes.*

3. Near whole-brain assessment of cortical depth dependent activity in resting-state fMRI

To investigate cross-layer interactions between distant cortical areas during rest, we acquired two additional task-negative fMRI scans from each subject, one using protocol-1, with 0.63 mm isotropic voxels, i.e., same as for the task-fMRI, and another using protocol-2, with higher in-plane resolution (0.51 × 0.51 mm^2) and thicker slices (1.00 mm) to maintain a reasonable SNR level. In order to reduce the dimensionality of our data (6 surfaces × ~ 290 000 vertices per hemisphere), we first segmented the cerebral cortex into 21 ROIs related to well-known brain networks: default mode, visual, sensory-motor, auditory, executive control and salience (**Fig. 4a** and **Table 1**). Having averaged the vertices within each ROI and each cortical layer in both cerebral hemispheres, we obtained 252 time courses from each fMRI scan (21 ROIs × six surfaces × two hemispheres). These were then subjected to several analysis methods. Following an amplitude-frequency decomposition of the functional time courses, it was found that most cortical areas exhibit a higher level of activity in their superficial layers (**Fig. 4c**). This activity was observed to oscillate mostly within the range 0.01-0.03 Hz, which is in agreement with other non-laminar rs-fMRI studies focusing on cortical gray matter [59-62]. Integration of the signals fluctuating between 0.01 and 0.1 Hz, i.e., the typical range considered in rs-fMRI studies [63], provided a simplified measure of brain activity during rest, commonly denoted as the amplitude of low-frequency fluctuations (ALFF), which was assessed for each ROI and the six different cortical depths. **Figure 4d** shows the dependence of resting-state activity on cortical depth for each cerebral hemisphere. The level of activity was observed to increase towards the surface of the cortex in most ROIs, irrespective of whether these were assessed in cortical gyri or cortical sulci (**Fig. 4d**). Similarly, when ROIs were grouped into functional networks, a higher average ALFF was observed in more superficial layers, with the visual network and the auditory network exhibiting the most and the least inclined laminar gradient, respectively (**Fig. 4e**: "slope" inset). Although finer evaluation of the rs-fMRI signal, e.g., targeting smaller areas, may identify more specific roles of the deep cortical layers (e.g., [64]), the ALFF assessment based on 21 ROIs suggested that the superficial layers in the cortex play a major factor in the maintenance of resting-state activity.

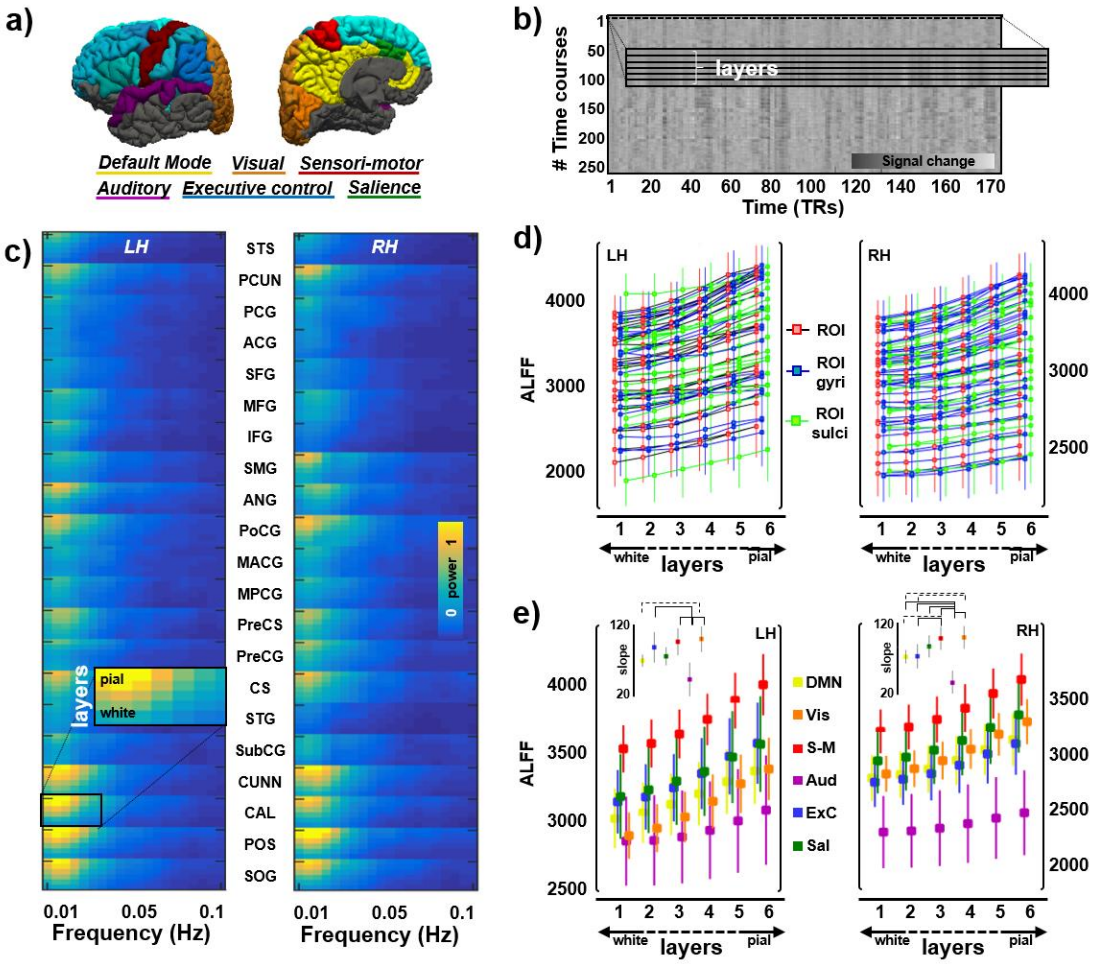

Figure 4. Cortical depth-dependent resting-state activity. a) *The figure displays the regions that were included in the functional analysis, organized by network, over the surface of the brain (see* ***Table 1*** *for a detailed description of the ROIs included).* ***b)*** *An example of all of the time courses (amplitude color-coded in gray-scale) to be evaluated from a 10 min scan conducted at rest. In total, 252 time courses were extracted, which result from averaging the time courses of all vertices within each ROI and each cortical surface, for each cerebral hemisphere.* ***c)*** *Mean layer-specific frequency-power decomposition of the BOLD signal in 21 ROIs (both cerebral hemispheres), averaged across 18 subjects.* ***d)*** *The plot shows the cortical depth dependence of the resting-state activity, measured as average ALFF, through all ROIs and both cerebral hemispheres (each set of line-connected dots has been extracted from a different ROI). Different colors indicate whether the ROI was considered in its entirety ("ROI"), whether only the vertices corresponding to the gyri in each ROI were considered ("ROI in gyri"), or whether only the vertices corresponding to the sulci in each ROI were considered ("ROI in sulci").* ***e)*** *ALFF averaged within the ROIs of 6 functional networks. The inset on the top left area of each graph provides the slope of the fitting line that approaches best the depth-varying ALFF for each cortical network. Error bars represent standard error of the mean. Horizontal lines above the graph indicate significant differences between the slope of functional networks (p-value < 0.05 for dashed lines and < 0.01 for solid lines).*

In addition to using ALFF to assess the "amount" of brain activity during rest, we investigated the connections between different brain regions at different depths of the cerebral cortex. To do so, a functional connectivity matrix was generated from each fMRI scan, which included the temporal correlation between all pairs of time courses, i.e., between the average time course of each region at each layer and that of every other region and layer (i.e., 252^2 cells). **Figure 5a** shows the connectivity matrix from a representative subject. The correlation values of the six layers in each ROI and the six layers of every other ROI were computed. For group analysis, the connectivity matrices of 17 subjects were averaged and subjected to a t-test for statistical thresholding. The resulting adjacency matrix was then used to generate a layer-specific, whole-brain connectivity graph. This was done for each scan acquired (**Fig. S3d, S3i & S3n)**. In order to simplify the connectivity results, inter-regional connections were grouped per network. **Figure 5d-f** shows three versions, with variable layer visibility, of four connectivity graphs demonstrating the depth-specific connections within the default mode network, the executive control network, the visual network and the sensory-motor network, obtained from a resting-state scan acquired with protocol-1 (N=17). The same graphs were also computed from the task-based fMRI obtained with protocol-1 and the rs-fMRI obtained with protocol-2, which can be found in **Figure S4**. From a global-ROI perspective, i.e., independent of cortical depth, our data showed reliable connections that are in agreement with the volume-based resting-state network results derived from an ICA analysis; the volume-based examples and the corresponding depth-dependent profiles per ROI are shown in **Fig. 5g** and **Fig. S5**, respectively. To facilitate the visual inspection of the depth-dependent connectivity graphs, the six assessed layers were grouped into "deep" (white + layer02), "intermediate" (layer04 + layer06) and "superficial" layers (layer08 + pial), and connections were color-coded based on the pair of cortical depths involved, e.g., deep–deep connections were represented by yellow lines, intermediate–intermediate connections by red lines, deep-intermediate connections by orange lines, etc. Overall, long-range functional connections were mostly observed between superficial and middle layers, but some statistically significant correlations were also observed involving deeper cortical layers (**Fig. 5d-f**). The similarity between the layer-specific connectivity graphs obtained from rs-fMRI using protocols 1 and 2 (**Fig. S3 and S4)** suggests that the TR-external EPIK sequence is a high reliability method for mapping cortical connections through the brain. Furthermore, the differences in the connectivity graphs obtained from the fMRI scans acquired with protocol-1 during rest or task performance, i.e., the general decrease of the connectivity of resting-state networks during a motor task (**Fig. S3i**), also demonstrates the sensitivity of TR-external EPIK for tracking brain state changes.

The connections between each layer in the brain are summarized in three connectivity matrices showing the average correlation between the layers of the ROIs in the left hemisphere (**Fig. 5b**, "Within LH"), the right hemisphere (**Fig. 5b**, "Within RH"), and the average inter-hemispheric correlation, i.e., layers of ROIs in the left hemisphere connecting with layers of ROIs in the right hemisphere (**Fig. 5b**, "Inter-hemispheric"). These matrices further suggested that the superficial two-thirds of the cerebral cortex are strongly involved in maintaining both intra- and interhemispheric connectivity. Note that the average connectivity between reciprocal layers (diagonal elements) was higher between hemispheres, possibly reflecting the connectivity between counterpart layers in opposite hemispheres. Similarly, when evaluating the ROI-specific connectivity per cortical depth (considering both, intra and inter-hemispheric connectivity), all of the ROIs evaluated

exhibited their maximum values at the intermediate or superficial layers of the cortex (**Fig. 5c**). The assessment of the cortical depth-dependent global connectivity for each network (**Fig. 5h-j**) further verified the presence of a positive cortical connectivity slope, i.e., superficial layers more connected than deep layers, within all resting state networks, which was largest for the visual network (**Fig. 5j**). A connectivity analysis based on coherence instead of temporal correlation showed similar results (**Fig. S6**). These findings are in agreement with previous reports demonstrating a higher level of activity and communication near the surface of the cortex in humans and non-human primates during rest [64, 65].

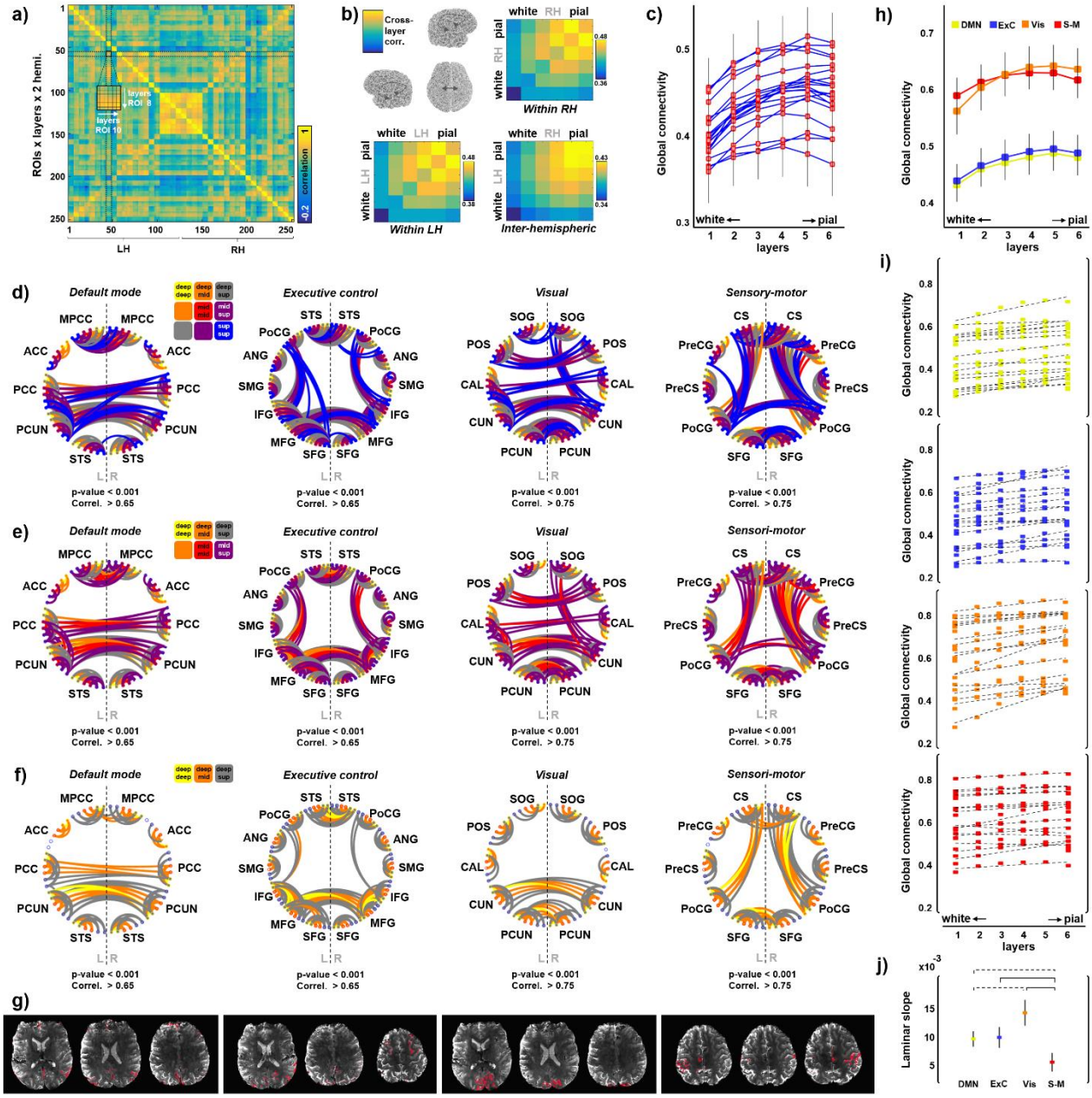

Figure 5. Cortical depth-dependent functional connectivity. a) *Representative connectivity matrix integrating the temporal correlation values between six cortical layers of 21 ROIs in both cerebral hemispheres.* ***b)*** *Average cross-layer connectivity within and between hemispheres.* ***c)*** *Depth-dependence of global connectivity in 21 cortical ROIs.* ***d)*** *Four graphs showing the layer-specific functional connections between ROIs engaged in four different brain networks. A legend is provided above the first graph. Note the marked predominance of*

*pial-pial connections over the brain. A version of these graphs hiding the top two superficial layers (i.e., only deep and intermediate layers are visible) and the two middle layers (i.e., only deep layers are visible) is provided in **e)** and **f)**, respectively. **g)** Below each set of connectivity graphs, three representative axial slices showing a volume-based ICA identification of the particular network are presented. In the case of the sensory-motor network, the three independent components reflecting left, bilateral and right sensory-motor network are shown. **h)** Depth-dependent global connectivity assessed in four functional networks. **i)** Each of the four graphs shows the averaged connectivity for each functional network at each cortical depth for all subjects included in the analysis. Each dash line is the result of a linear fitting for one subject's data. **j)** Average slope of the fitting lines in i). Horizontal lines above the graph indicate significant differences between the slope of functional networks (p-value < 0.05 for dashed lines and < 0.01 for solid lines). Error bars indicate ± standard error of the mean. N=17 for all group results.*

Concerned that our results highlighting the role of superficial layers may simply reflect a surface-vein-related bias, we conducted an additional assessment in three separate regions that are presumably engaged in motor processing. Specifically, we extracted small patches from the primary motor cortex (M1), lateral premotor cortex (PreM) and supplementary motor area (SMA), as shown in **Fig. 6**. Rather than measuring temporal correlation, we evaluated the coherence between each pair of the layer-specific time courses, which reflects the similarity of both signals in terms of their frequency content. In this way, it was possible to obtain a measure less biased by particular events in time [62, 66, 67]. In agreement with our previous results, we found higher coherence values between the superficial layers of the three cortical regions during rest (**Fig. 6a**, 2nd leftmost column). However, when the same layer-specific inter-regional coherence was evaluated during the performance of a motor task, the relationship between areas appeared disrupted (**Fig. 6a**, rightmost column), especially between M1 and PreM, demonstrating a layer-specific preference in frequency-based communication during motor engagement. A summary of the coherence-based relationship between the cortical layers in M1, PreM and SMA during resting state and during task performance is presented in **Fig. 6b**. The evaluation of this simplified circuit with analysis methods based on temporal correlation instead of coherence also identified a slightly altered pattern in the task fMRI scan, but its deviation from the typical top-down profile observed during rest was much less apparent (**Fig. S7**, bottom middle panel). The discrepancies found between resting-state and task-performance layer-to-layer coherence suggest that TR-external EPIK is capable of tracking layer-specific functional changes associated to brain state switches.

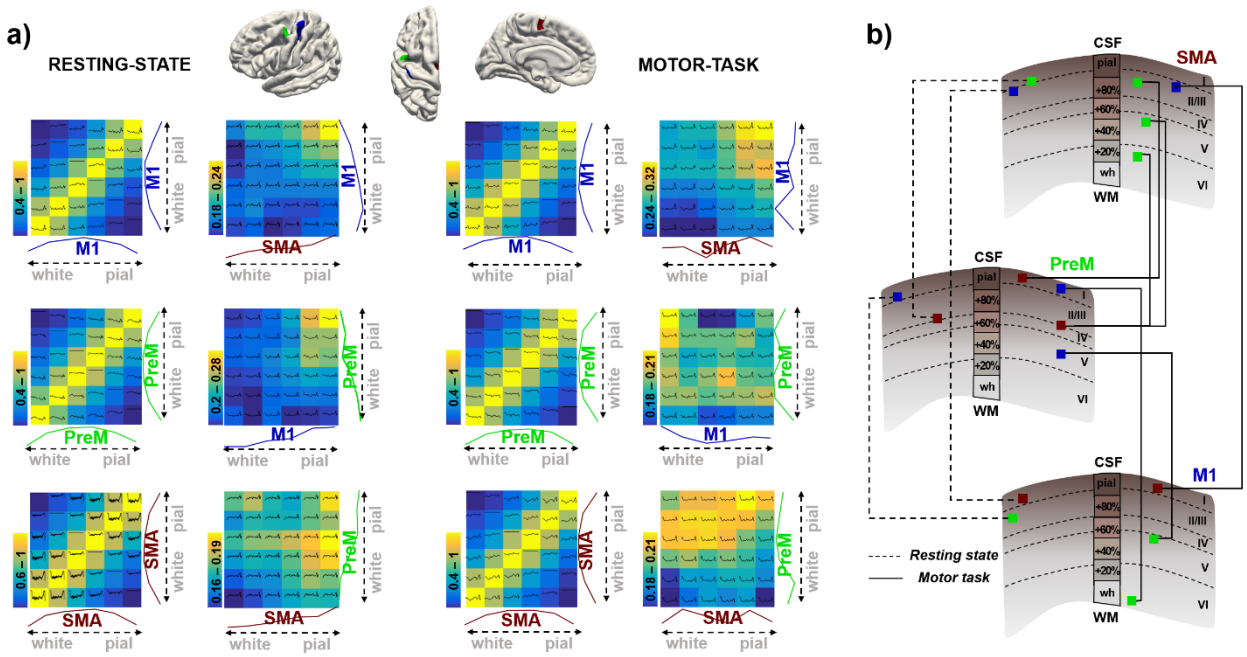

Figure 6. Coherence between cortical laminae of the motor system. a) *Coherence matrices calculated from rs-fMRI (left set of matrices, N=17) and motor-task fMRI data (right set, N=17) for 3 ROIs involved in motor function. The location of the selected ROIs is displayed over a pial surface reconstruction of the brain (fsaverage). For each pair of ROIs, the average depth-dependent coherence is shown color-coded in a six layer × six layer matrix. Overlaid on each cell is the average coherence through frequencies 0.001-0.15 Hz. The plots on the bottom and right side of each matrix represent the laminar coherence profile (average coherence per layer) for each of the two ROIs. Note the more heterogeneous coherence between ROIs during a motor-task (right set of matrices).* ***b)*** *Main inter-ROI connections between primary motor cortex (M1), lateral premotor cortex (PreM) and supplementary motor area (SMA), based on their average coherence, summarized from the results in a). In each of the three cortical sketches, the approximate location of the histological layers is indicated in dashed lines, with the artificially generated layers used in our study shown in the center as boxes (equally distributed along the cortical thickness).*

DISCUSSION

Despite the growing body of literature focusing on fMRI-based assessment and modeling of cortical behavior in the human brain [15, 16, 18-22, 28, 38, 68-72], the cortical depth specificity of current imaging schemes has usually been limited to restricted FOVs, e.g., the motor cortex, the visual cortex, etc., due to the technical limitations of the fMRI sequences employed. Hence, the layer-specific communication patterns across distant brain regions remain largely unexplored. We have recently developed a laminar-compatible (voxel size ~ 0.25 mm^3) fMRI sequence, termed TR-external EPIK [49], that is able to preserve near whole-brain coverage and has comparatively low distortion behavior at 7T. In this report, we demonstrate its suitability for mapping whole-brain activity with cortical depth specificity. We show that the observed motor-evoked responses in M1 reproduce the laminar results seen in the existing literature and we further provide a three-way characterization of the resting-state signals from different regions, in terms of layer-specific frequency content, functional connectivity, and coherence.

We acquired two sets of rs-fMRI data: one using isotropic voxels and the other using higher in-plane spatial resolution but with thicker slices. Both sets of data had voxels of similar volume (~ 0.25 mm^3). The resemblance between the power spectrum, connectivity and coherence assessed in both sets of the rs-fMRI data suggests that both protocols were able to detect brain connectivity with layer-specificity to a similar level of performance. In both cases, the superficial layers exhibited the largest activity fluctuations, higher temporal correlations and most salient coherence values. Despite the agreement between both protocols, protocol-2 was better able to detect statistically significant connections (**Fig. S3n** compared to **S3d**) and gave a higher magnitude of the assessed responses (**Fig. S3k** compared to **S3a**). This was possibly due to the increased SNR afforded by protocol-2 [49]. Moreover, protocol-2 conferred more complete brain coverage, which may be critical for particular applications where structures that are located at the base of the brain, e.g., hippocampus, brainstem, etc., are significant for the integrity of the study. Therefore, despite the non-isotropic voxel dimensions of protocol-2 (0.51 × 0.51 × 1.00 mm), it may be a better candidate than protocol-1 for whole-brain laminar fMRI. A more detailed technical description of both of the TR-external EPIK protocols can be found in reference [49].

In previous literature, a higher activation of superficial, i.e., supragranular, cortical layers has been observed in laminar rs-fMRI studies that have focused on a restricted FOV in the human brain [64], in non-human primates [65], and in rodents [73]. In contrast to the granular layer, which receives thalamo-cortical afferents, and the deeper, i.e., infragranular, layers, which mainly initiate efferent responses through subcortical and spinal projections, the superficial layers are the principal source and target of cortico-cortical regulatory communication [74-79]. Hereby, the deeper portion of layer III receives long distance feedforward projections, whereas its superficial portion, together with layer II, is targeted by long-distance feedback projections [39]. The present results support the supposition that superficial layers play a role in resting-state maintenance, as resting-state networks mostly involve cortical areas [41, 80]. Although the literature upholds the results obtained from our resting-state analysis, i.e., predominant participation of the superficial layers, the GE nature of the sequence employed poses questions as to whether the recorded signal could be merely a reflection of a vascular-related superficial bias. To rule this possibility out, we performed a coherence analysis in small areas of the cortex in two resting-state paradigms and in one motor task. While the resting-state data exhibited a superficial dominance, the task-related coherence yielded certain heterogeneous profiles involving specific layer-to-layer interactions (**Fig. 6**). Therefore, a vein-related bias, if present, was not the only factor accounting for the observed responses. Notwithstanding this assertion, the potential implications of using a GE-based sequence will be discussed below.

In comparison to the resting-state paradigm, the assessment of layer-specific correlations during task performance revealed a decreased number of functional connections (**Fig. S3i** vs. **S3d**), which is in agreement with the literature [81]. In contrast to the decreased functional connectivity of broad networks, the signal fluctuation in the left precentral gyrus exhibited higher power during task performance compared to rest (**Fig. S3f** vs. **S3a**, red rectangle), which is consistent with a more active primary motor cortex. The specificity of the

evoked responses was demonstrated with distinct line profiles in the precentral gyrus, in response to somatomotion, with and without somatosensation (**Fig. 3l**). Finger movement resulted in activation of the superficial and, to a lesser extent, deeper layers, the latter possibly indicating signaling from premotor and supplementary motor cortices, also coinciding with cortical motor efferents towards pontomedullary or thalamic nuclei [73, 82]. Sensory processing triggered by touch between two digits produced activation in intermediate layers, possibly reflecting the modulation of the motor cortex by sensory cortical areas and afferents from the sensory thalamus [73, 82, 83]. The activation observed near the cortical surface may reflect, at least to a certain extent, a contribution from the venous network. However, superficial neuronal responses can be expected during performance of a motor task, as motor thalamic afferents modulate motor behavior in superficial and intermediate layers of the cortex, in a similar way as the sensory thalamic afferents upon addition of touch [82]. The fact that evoked responses in the intermediate and deep layers (**Fig. 3j**) were detected in a line-profile analysis but not in the analysis of a bigger cortical patch, also responding to the motor task but exhibiting an upper → deeper trend only, demonstrates the specificity of the laminar responses and the overall preponderance of BOLD responses in the superficial layers.

Assuming a fair neuro-vascular coupling, the fMRI signal extracted from a cortical capillary network is a reliable indicator of neuronal activity. However, capillaries supplying blood to neurons flow in bigger ascending venules that run perpendicular to the cortex and disgorge into pial veins tangential to the surface of the brain, and these veins influence the fMRI signal and can result in a bias towards the superficial layers of the cortex. The current study is based on GE-BOLD fMRI, which is known to be sensitive to changes in the macrovasculature; hence, it presents a less spatially-specific signal than other acquisition schemes, such as SE-BOLD fMRI, sensitive to oxygenation changes in the microvasculature only, vascular space occupancy fMRI (VASO), sensitive to vessel dilation, or cerebral blood flow-based fMRI (CBF), sensitive to flow changes. Due to the short T2 constant of blood at ultra-high field, BOLD-fMRI at 7T is only sensitive to the extra-vascular effect of the oxy/deoxy-hemoglobin ratio, in vessels of all sizes. Although the parenchymal vessels, i.e., venules of diameter < 25 μm, are detected by both SE- and GE-BOLD, these are often overshadowed in GE sequences by the influence of bigger veins running along the surface of the brain, which cause static perturbations in the magnetic field affecting the neighboring parenchymal tissue. Therefore, while SE-BOLD offers a fine localization of the activated parenchyma, GE-BOLD provides a mixed signal that is relevant to both small parenchymal vessels and macroscopic veins. To correct for this bias, we subtracted the time-varying phase component of the MR signal from each voxel's magnitude time course. The time-varying phase component is proportional to the frequency offset exhibited by the spins and hence, sensitive to the venous vasculature [29, 30]. As large vessels produce field inhomogeneities, spins precessing in the neighboring parenchyma would produce changes in the phase component of the signal; in contrast, small randomly oriented vessels, e.g., in the capillary network within the gray matter, do not produce a net phase and hence, their derived signal remains intact. Although this method helps to improve the local specificity of BOLD, several biases could remain in the corrected data, such as those derived from motion correction or geometric distortions [84]; it is worth noting that the last ones are generally reduced in EPIK compared to conventional EPI [51].

Additionally, the frequency offsets derived from field inhomogeneities around vessels that are oriented parallel to the B0 field cannot be compensated for during the post-processing [85]. A few groups have demonstrated the dependence of laminar fMRI on the orientation of the cortex with respect to B0 [85, 86]. Although orientation bias can be critical for the dissection of the fMRI signal, this effect has been correlated with low frequency drift, motion and respiratory cycles, which were accounted for in our study, therefore diminishing the discussed effect. Moreover, most of our results were obtained from relatively big patches of cortex and through multiple ROIs, averaging vertices with different orientations within a cortical surface, and hence, although non-negligible, an orientation bias is not expected to have conditioned our results. However, a future model accounting for such an effect could determine the extent to which the curvature affects the laminar profiles at a whole-brain level.

In contrast to retrospective model-based approaches that reduce the superficial BOLD bias by applying temporal decomposition [35], linear detrending [31], normalization [32] or deconvolution [33, 34] to evoked fMRI data, the phase-based correction method employed here does not involve a priori assumptions about the behavior of the vascular dynamics across the cortical thickness and does not rely on the use of an evoked paradigm, offering a bias-free alternative to correct resting-state GE-fMRI data. Based on our results, this phase-based method [29] may constitute a rather conservative approach, i.e., despite the laminar differences tracked across cortical areas and networks, the activity of the superficial layers was found to predominate in most measures assessed. Future studies comparing GE-EPIK and SE-EPIK activation profiles will investigate the possibility of complementing the phase-correction method with additional strategies to exploit the high SNR of GE-schemes with robust laminar specificity.

The vascular dependence of the fMRI signal remains one of the biggest challenges in laminar fMRI [87]. Signals obtained with BOLD contrast are not only conditioned by a physically-constrained laminar point-spread function, i.e., the fact that ascending venules spread the deep activation signals towards superficial layers [34, 88, 89], but also by the varying physiological mechanisms underlying the BOLD response (CBF, CMRO2, CBV), which can modulate this point-spread function across cortical layers [88]. Despite the complexity of the model, laminar fMRI studies have even employed strategies that artificially sample the cortical depth with a number of points higher than the number of voxels across the cortical ribbon. This is appropriate under the assumption that the purpose of the study is tracking the trend of activation across the cortical depth and not to resolve the actual neuronal signal at any particular layer, which is indeed not possible, even with sufficient spatial resolution, given the facts discussed above. In this study, the number of depths used was equal to the number of histologically-defined layers in the neocortex; however, the layers in our model have been arbitrarily chosen to be equally spaced along the cortical thickness and have no direct relationship with the cortical cytoarchitecture, hence, our conclusions should be interpreted in terms of cortical depth only. Although some reports have chosen a smaller number of layers for their laminar assessment (e.g., 3 [43]), which simplifies the analysis and confers layers with a greater independence, others have shown that a greater number of depths (e.g., 20 [16]), enables clearer detection of cortical responses, despite the fact that this strategy involves a greater dependence on neighbor signals. In addition, the last scheme also poses an important

challenge in whole-brain studies due to the high computational demands of the analysis procedure (see discussion below).

Irrespective of the number of layers, ambitious whole-brain laminar fMRI studies should assure perfect co-registration between the anatomical reference scan and the functional data. Previous reports have shown the possibility of integrating T1 contrast within a high-resolution fMRI sequence (e.g., [16], acquired during VASO), which allows a 1:1 relationship between the anatomical and functional scans, mitigating any co-registration concern. This option was not yet available in the current study. Nevertheless, in this work, we achieved acceptable co-registration in the majority of the brain by using manual rigid transformations (**Fig. S8**), which proved to be more reliable than the transformations rendered by non-linear automatic registration tools. In addition, the improved robustness against geometric distortions in EPIK [51] is expected to yield fewer co-registration errors, compared to the common EPI, between the functional scans and the anatomical scans (e.g., MR2RAGE). However, particular areas in different subjects remained poorly co-registered and needed to be masked out to ensure a proper laminar analysis. In the future, TR-external EPIK will be modified to provide a T1 contrast, which will avoid data loss, reduce the pre-processing time and, more importantly, will alleviate the potential concerns relating to co-registration.

In this work, we employed TR-external EPIK to map the majority of the brain with a voxel resolution of 0.63 × 0.63 × 0.63 mm^3 or 0.51 × 0.51 × 1.00 mm^3. In addition to the challenge in terms of sequence design, the resulting matrix size imaged by TR-external EPIK (336 × 336 × 123 or 408 × 408 × 108) presents important computational limitations, such as the relatively large memory required (minimum storage space: ~ 6 Gb per 4D-volume; RAM: ≥ 32Gb for many pre-processing steps) and long processing times. After pre-processing, analysis of the cortical surfaces with numerical computing environments such as Matlab is, again, conditioned by the number of vertices to be processed, and therefore, the greater the number of layers, the higher the computational demands. For instance, one cortical surface covered by protocol-1 contained ~ 290,000 vertices, which means that the six surfaces obtained from both hemispheres involved the analysis of ~ 3,480,000 vertices, each of them consisting of a 172-point time course. In this work, in order to adjust the computational demands to those of a standard scientific workstation, the first step in most of the layer-specific functional analysis was to average all vertices specific to one layer within one ROI. Given that the laminar performance of the cortex can be highly localized, some events might be overlooked when using an ROI-based analysis to identify particular behaviors; hence, the use of supercomputing resources to assess vertex-specific measures becomes highly desirable to exploit the capabilities of the acquired data.

CONCLUSION

This study adopted a sequence offering exceptional resolution (~ 0.25 mm^3 voxels) to map laminar functional dynamics in a 7T scanner with near whole-brain mapping in healthy volunteers. We investigated the dependence of common rs-fMRI measures such as ALFF, functional connectivity and the coherence of brain networks on cortical depth, which has emerged as a new dimension to be explored in the human brain and

suggests that the superficial layers play a critical role in the maintenance of the resting-state. In the future, the employed sequence (TR-external EPIK) will be modified to include SE-BOLD contrast, to avoid any GE-related bias, and T1-contrast, to ensure perfect co-registration between functional and anatomical volumes. This work sets the basis for novel investigations of the resting-state in particular in neuro-psychological diseases with cortical depth specificity.

METHODS

Subjects:

Eighteen healthy volunteers (14 males and 4 females; age, 23-47 years; 17/18 right-handed, 1/18 left-handed [90]) participated in this study. The experimental methods were approved by the local institutional review board (EK 346/17, RWTH Aachen University, Germany). MR-safety screening was performed on all subjects prior to MRI acquisition and informed written consent was obtained from all volunteers. Subjects were scanned in one single session for a period of ~55 min, which included two resting-state fMRI scans (rs-fMRI), one finger motor task fMRI scan (task-fMRI) and an MP2RAGE scan. A pneumatic belt was positioned around the subject's chest, and a pulse oximeter was placed on the 2nd, 3rd, or 4th finger of the left hand in 16 subjects to control for potential interference of the physiological signals on the fMRI responses [91].

Experimental design:

In the rs-fMRI, subjects were asked to remain still, awake, with eyes closed and without thinking about anything in particular. In total, 172 volumes were acquired during the rs-fMRI (~10 min). For task-fMRI, subjects were asked to follow instructions on a projected screen and to perform flexion of the right index finger, without necessarily touching the thumb. The task was performed continuously at a comfortable pace (1-2 Hz, for most subjects) for 21 s and was repeated 12 times, alternated with 21 s of rest. In total, 148 volumes were obtained (4 s rest, [21 s task, 21 s rest] × 12) (~ 8,6 min). One subject was invited to participate in an additional scan session and first performed a finger motor task (4 s rest, [21 s task, 21 s rest] × 8), followed by a finger motor and sensory task, i.e., instructions were given to approach the right index finger towards the thumb involving touching (4 s rest, [21 s task, 21 s rest] × 8).

MRI data acquisition:

MRI data were collected on a Siemens Magnetom Terra 7T scanner with a 1-channel Tx / 32-channel Rx Nova Medical head coil. An anatomical MRI volume was acquired using an MP2RAGE sequence, TR/TE = 4300/2 ms, matrix = 256 × 376 × 400 (0.60 × 0.60 × 0.60 mm^3). Functional MRI data were obtained using gradient-echo EPI with keyhole (EPIK) combined with a TR-external EPI phase correction scheme (the sequence performance has been previously described elsewhere [49]), using two different acquisition protocols. In both protocols, TR/TE = 3500/22 ms, FA = 85°, partial Fourier = 5/8, 3-fold in-plane/3-fold inter-plane (multi-band) acceleration. B0 shimming was performed with a standard routine provided by the manufacturer. For protocol-1, matrix = 336 × 336 × 123 slices (0.63 × 0.63 × 0.63 mm^3). For protocol-2, matrix = 408 × 408 × 105 slices (0.51 × 0.51 × 1.00 mm^3). The main figures show results acquired with protocol-1 (i.e., isotropic voxels).

Data analysis:

A summarized pipeline of our pre-processing methods can be found in **Figure 1**. Briefly, cortical surfaces were extracted from the anatomical scan and used as a template to map the functional signals using Freesurfer (Martinos Center for Biomedical Imaging, Charlestown, MA). The average time course of 21 ROIs were extracted from each surface. Post-processing analysis included ICA-analysis, temporal correlation (i.e. functional connectivity) analysis, spectral decomposition, ALFF, coherence and surface GLM. The assessment of the cortical model (results in **Fig. 2**) is based on an excellent work by Kay et al. [28] Pre-processing was done mainly on AFNI (Analysis of Functional NeuroImages, NIH, Bethesda, MD), and post-processing software included FSL (FMRIB Software Library, Oxford, UK), AFNI and Matlab (Mathworks, Natick, MA).

Note that the term "surfaces" or "layers" employed through the manuscript should not be interpreted as histologically-defined cortical layers; instead, the terms are employed to refer to each of the six different cortical depths that are artificially generated by splitting the cortical thickness into five different compartments. See *Supplementary Methods* for details.

ACKNOWLEDGEMENTS

We thank Dr Michael Schwerter for guidance in the phase-signal processing; Ms Elke Bechholz and Ms Anita Köth for technical support; Ms Rick Claire, for manuscript corrections, and the fMRI volunteers for their excellent cooperation.

Table 1. Regions of interest.

Abb. ROI	Full ROI name	Related network(s)
MPCC	Middle-Posterior Cingulate	DMN
ACC	Anterior Cingulate	DMN
PCC	Posterior Cingulate	DMN
PCUN	Precuneus	DMN & VISUAL
STS	Superior Temporal Sulcus	DMN & EXEC
PoCG	Post-Central Gyrus	EXEC & SM
ANG	Inferior Parietal - angular	EXEC
SMG	Inferior Parietal - supramarginal	EXEC
IFG	Inferior Frontal G&S	EXEC
MFG	Middle Frontal Gyrus	EXEC
SFG	Superior Frontal G&S	EXEC & SM
SOG	Superior Occipital Gyrus	VISUAL
POS	Parieto-occipital Sulcus	VISUAL
CAL	Calcarine	VISUAL
CUN	Cuneus	VISUAL
CS	Central Sulcus	SM
PreCG	Pre-Central Gyrus	SM
PreCS	Pre-Central Sulcus	SM
STG	Superior Temporal Gyrus	AUDITORY
SubCG	Subcentral G&S	AUDITORY
MACG	Middle-Anterior Cingulate	SALIENCE

Table 1. DMN: default mode network; EXEC: executive control network; SM: sensory-motor network.

References:

1. Palomero-Gallagher, N. and K. Zilles, *Cortical layers: Cyto-, myelo-, receptor- and synaptic architecture in human cortical areas.* Neuroimage, 2019. **197**: p. 716-741.
2. Thomson, A.M. and A.P. Bannister, *Interlaminar connections in the neocortex.* Cereb Cortex, 2003. **13**(1): p. 5-14.
3. Larkum, M.E., et al., *A Perspective on Cortical Layering and Layer-Spanning Neuronal Elements.* Front Neuroanat, 2018. **12**: p. 56.
4. Michelson, N.J. and T.D.Y. Kozai, *Isoflurane and ketamine differentially influence spontaneous and evoked laminar electrophysiology in mouse V1.* J Neurophysiol, 2018. **120**(5): p. 2232-2245.
5. Krupa, D.J., et al., *Layer-specific somatosensory cortical activation during active tactile discrimination.* Science, 2004. **304**(5679): p. 1989-92.
6. Adesnik, H. and A. Naka, *Cracking the Function of Layers in the Sensory Cortex.* Neuron, 2018. **100**(5): p. 1028-1043.
7. Ayaz, A., et al., *Layer-specific integration of locomotion and sensory information in mouse barrel cortex.* Nat Commun, 2019. **10**(1): p. 2585.
8. Scott, B.B., et al., *Imaging Cortical Dynamics in GCaMP Transgenic Rats with a Head-Mounted Widefield Macroscope.* Neuron, 2018. **100**(5): p. 1045-1058 e5.
9. Csercsa, R., et al., *Laminar analysis of slow wave activity in humans.* Brain, 2010. **133**(9): p. 2814-29.
10. Logothetis, N.K., et al., *Neurophysiological investigation of the basis of the fMRI signal.* Nature, 2001. **412**(6843): p. 150-7.
11. Logothetis, N.K., *The neural basis of the blood-oxygen-level-dependent functional magnetic resonance imaging signal.* Philos Trans R Soc Lond B Biol Sci, 2002. **357**(1424): p. 1003-37.
12. Ogawa, S., et al., *Brain magnetic resonance imaging with contrast dependent on blood oxygenation.* Proc Natl Acad Sci U S A, 1990. **87**(24): p. 9868-72.
13. Yu, X., et al., *Deciphering laminar-specific neural inputs with line-scanning fMRI.* Nat Methods, 2014. **11**(1): p. 55-8.
14. Lawrence, S.J.D., et al., *Laminar fMRI: Applications for cognitive neuroscience.* Neuroimage, 2019. **197**: p. 785-791.
15. Guidi, M., et al., *Lamina-dependent calibrated BOLD response in human primary motor cortex.* Neuroimage, 2016. **141**: p. 250-261.
16. Huber, L., et al., *High-Resolution CBV-fMRI Allows Mapping of Laminar Activity and Connectivity of Cortical Input and Output in Human M1.* Neuron, 2017. **96**(6): p. 1253-1263 e7.
17. Chai, Y., et al., *Integrated VASO and perfusion contrast: A new tool for laminar functional MRI.* Neuroimage, 2020. **207**: p. 116358.
18. Huber, L., et al., *Cortical lamina-dependent blood volume changes in human brain at 7 T.* Neuroimage, 2015. **107**: p. 23-33.
19. Ress, D., et al., *Laminar profiles of functional activity in the human brain.* Neuroimage, 2007. **34**(1): p. 74-84.
20. Polimeni, J.R., et al., *Laminar analysis of 7T BOLD using an imposed spatial activation pattern in human V1.* Neuroimage, 2010. **52**(4): p. 1334-46.
21. Kashyap, S., et al., *Resolving laminar activation in human V1 using ultra-high spatial resolution fMRI at 7T.* Sci Rep, 2018. **8**(1): p. 17063.
22. van Mourik, T., et al., *Laminar signal extraction over extended cortical areas by means of a spatial GLM.* PLoS One, 2019. **14**(3): p. e0212493.
23. De Martino, F., et al., *Frequency preference and attention effects across cortical depths in the human primary auditory cortex.* Proc Natl Acad Sci U S A, 2015. **112**(52): p. 16036-41.
24. Lu, H., et al., *Functional magnetic resonance imaging based on changes in vascular space occupancy.* Magn Reson Med, 2003. **50**(2): p. 263-74.

25. Huber, L., et al., *Ultra-high resolution blood volume fMRI and BOLD fMRI in humans at 9.4T: Capabilities and challenges.* Neuroimage, 2018. **178**: p. 769-779.
26. Poplawsky, A.J., et al., *Layer-Specific fMRI Responses to Excitatory and Inhibitory Neuronal Activities in the Olfactory Bulb.* J Neurosci, 2015. **35**(46): p. 15263-75.
27. Zhao, F., P. Wang, and S.G. Kim, *Cortical depth-dependent gradient-echo and spin-echo BOLD fMRI at 9.4T.* Magn Reson Med, 2004. **51**(3): p. 518-24.
28. Kay, K., et al., *A critical assessment of data quality and venous effects in sub-millimeter fMRI.* Neuroimage, 2019. **189**: p. 847-869.
29. Menon, R.S., *Postacquisition suppression of large-vessel BOLD signals in high-resolution fMRI.* Magn Reson Med, 2002. **47**(1): p. 1-9.
30. Curtis, A.T., R.M. Hutchison, and R.S. Menon, *Phase based venous suppression in resting-state BOLD GE-fMRI.* Neuroimage, 2014. **100**: p. 51-9.
31. Fracasso, A., et al., *Laminar imaging of positive and negative BOLD in human visual cortex at 7T.* Neuroimage, 2018. **164**: p. 100-111.
32. Kashyap, S., et al., *Impact of acquisition and analysis strategies on cortical depth-dependent fMRI.* Neuroimage, 2018. **168**: p. 332-344.
33. Heinzle, J., et al., *A hemodynamic model for layered BOLD signals.* Neuroimage, 2016. **125**: p. 556-570.
34. Markuerkiaga, I., M. Barth, and D.G. Norris, *A cortical vascular model for examining the specificity of the laminar BOLD signal.* Neuroimage, 2016. **132**: p. 491-498.
35. Kay, K., et al., *A temporal decomposition method for identifying venous effects in task-based fMRI.* Nat Methods, 2020. **17**(10): p. 1033-1039.
36. Siero, J.C., et al., *Cortical depth-dependent temporal dynamics of the BOLD response in the human brain.* J Cereb Blood Flow Metab, 2011. **31**(10): p. 1999-2008.
37. Muckli, L., et al., *Contextual Feedback to Superficial Layers of V1.* Curr Biol, 2015. **25**(20): p. 2690-5.
38. Yacoub, E., N. Harel, and K. Ugurbil, *High-field fMRI unveils orientation columns in humans.* Proc Natl Acad Sci U S A, 2008. **105**(30): p. 10607-12.
39. Zilles, K. and M. Catani, *Cerebral hemispheres*, in *Gray's Anatomy*. 2020.
40. Scheeringa, R., et al., *The relationship between oscillatory EEG activity and the laminar-specific BOLD signal.* Proc Natl Acad Sci U S A, 2016. **113**(24): p. 6761-6.
41. Raichle, M.E., et al., *A default mode of brain function.* Proc Natl Acad Sci U S A, 2001. **98**(2): p. 676-82.
42. De Martino, F., et al., *Whole brain high-resolution functional imaging at ultra high magnetic fields: an application to the analysis of resting state networks.* Neuroimage, 2011. **57**(3): p. 1031-44.
43. Sharoh, D., et al., *Laminar specific fMRI reveals directed interactions in distributed networks during language processing.* Proc Natl Acad Sci U S A, 2019. **116**(42): p. 21185-21190.
44. Huber, L., et al., *Layer-dependent functional connectivity methods.* Prog Neurobiol, 2020: p. 101835.
45. Shah, N.J., Zilles, K., *Verfahren zur Untersuchung eines Objektes mittels Erfassung des Ortsfrequenzraumes*. 2003.
46. Shah NJ, a.Z.K., *Imaging process in the spatial frequency space and useful for examining the properties of object*. 2004.
47. Zaitsev, M., K. Zilles, and N.J. Shah, *Shared k-space echo planar imaging with keyhole.* Magn Reson Med, 2001. **45**(1): p. 109-17.
48. Zaitsev, M., et al., *Dual-contrast echo planar imaging with keyhole: application to dynamic contrast-enhanced perfusion studies.* Phys Med Biol, 2005. **50**(19): p. 4491-505.
49. Yun, S., P. Pais-Roldán, and N.J. Shah. *Detection of Cortical Depth-dependent Functional Activation using Whole-brain, Half-millimetre Resolution EPIK at 7T*. in *ISMRM*. 2020. Paris, France.

50. Yun, S.D. and N.J. Shah, *Analysis of EPI phase correction with low flip-angle excitation to reduce the required minimum TE: Application to whole-brain, submillimeter-resolution fMRI at 3 T.* Magn Reson Med, 2020. **84**(3): p. 1416-1429.
51. Yun, S.D., et al., *Parallel imaging acceleration of EPIK for reduced image distortions in fMRI.* Neuroimage, 2013. **73**: p. 135-43.
52. Yun, S.D. and N.J. Shah, *Whole-brain high in-plane resolution fMRI using accelerated EPIK for enhanced characterisation of functional areas at 3T.* PLoS One, 2017. **12**(9): p. e0184759.
53. Caldeira, L.L., et al., *Dynamic susceptibility contrast parametric imaging using accelerated dual-contrast echo planar imaging with keyhole.* J Magn Reson Imaging, 2019. **50**(2): p. 628-640.
54. Shah, N.J., N.A. da Silva, and S.D. Yun, *Perfusion weighted imaging using combined gradient/spin echo EPIK: Brain tumour applications in hybrid MR-PET.* Hum Brain Mapp, 2019.
55. Yun, S.D., et al., *Evaluating the Utility of EPIK in a Finger Tapping fMRI Experiment using BOLD Detection and Effective Connectivity.* Sci Rep, 2019. **9**(1): p. 10978.
56. Yun, S. and N.J. Shah, *Full-FOV, Whole-brain, Half-millimetre Resolution fMRI at 7T using Accelerated multi-band EPIK with TR-external Phase Correction*, in *27th Annual Meeting of ISMRM*. 2019: Montreal, Canada.
57. von Economo, C. and G.N. Koskinas, *Die Cytoarchitektonik der Hirnrinde des erwachsenen Menschen.* Springer, 1925.
58. Geyer, S., et al., *Two different areas within the primary motor cortex of man.* Nature, 1996. **382**(6594): p. 805-7.
59. Zuo, X.N., et al., *The oscillating brain: complex and reliable.* Neuroimage, 2010. **49**(2): p. 1432-45.
60. Xue, S.W., et al., *Different neural manifestations of two slow frequency bands in resting functional magnetic resonance imaging: a systemic survey at regional, interregional, and network levels.* Brain Connect, 2014. **4**(4): p. 242-55.
61. Yuen, N.H., N. Osachoff, and J.J. Chen, *Intrinsic Frequencies of the Resting-State fMRI Signal: The Frequency Dependence of Functional Connectivity and the Effect of Mode Mixing.* Front Neurosci, 2019. **13**: p. 900.
62. Bajaj, S., et al., *Oscillatory motor network activity during rest and movement: an fNIRS study.* Front Syst Neurosci, 2014. **8**: p. 13.
63. Murphy, K., R.M. Birn, and P.A. Bandettini, *Resting-state fMRI confounds and cleanup.* Neuroimage, 2013. **80**: p. 349-59.
64. Guidi, M., et al., *Cortical laminar resting-state signal fluctuations scale with the hypercapnic blood oxygenation level-dependent response.* Hum Brain Mapp, 2020. **41**(8): p. 2014-2027.
65. Mishra, A., et al., *Functional connectivity with cortical depth assessed by resting state fMRI of subregions of S1 in squirrel monkeys.* Hum Brain Mapp, 2019. **40**(1): p. 329-339.
66. Sun, F.T., L.M. Miller, and M. D'Esposito, *Measuring interregional functional connectivity using coherence and partial coherence analyses of fMRI data.* Neuroimage, 2004. **21**(2): p. 647-58.
67. Li, K., et al., *Review of methods for functional brain connectivity detection using fMRI.* Comput Med Imaging Graph, 2009. **33**(2): p. 131-9.
68. van Dijk, J.A., et al., *Linear systems analysis for laminar fMRI: Evaluating BOLD amplitude scaling for luminance contrast manipulations.* Sci Rep, 2020. **10**(1): p. 5462.
69. Lawrence, S.J., D.G. Norris, and F.P. de Lange, *Dissociable laminar profiles of concurrent bottom-up and top-down modulation in the human visual cortex.* Elife, 2019. **8**.
70. Kok, P., et al., *Selective Activation of the Deep Layers of the Human Primary Visual Cortex by Top-Down Feedback.* Curr Biol, 2016. **26**(3): p. 371-6.
71. Huber, L., K. Uludag, and H.E. Moller, *Non-BOLD contrast for laminar fMRI in humans: CBF, CBV, and CMRO2.* Neuroimage, 2019. **197**: p. 742-760.

72. Huber, L., et al., *Sub-millimeter fMRI reveals multiple topographical digit representations that form action maps in human motor cortex.* Neuroimage, 2020. **208**: p. 116463.
73. Weiler, N., et al., *Top-down laminar organization of the excitatory network in motor cortex.* Nat Neurosci, 2008. **11**(3): p. 360-6.
74. Moerel, M., et al., *Processing complexity increases in superficial layers of human primary auditory cortex.* Sci Rep, 2019. **9**(1): p. 5502.
75. D'Souza, R.D. and A. Burkhalter, *A Laminar Organization for Selective Cortico-Cortical Communication.* Front Neuroanat, 2017. **11**: p. 71.
76. Rubio-Garrido, P., et al., *Thalamic input to distal apical dendrites in neocortical layer 1 is massive and highly convergent.* Cereb Cortex, 2009. **19**(10): p. 2380-95.
77. Larkum, M.E., *The yin and yang of cortical layer 1.* Nat Neurosci, 2013. **16**(2): p. 114-5.
78. Sempere-Ferrandez, A., S. Martinez, and E. Geijo-Barrientos, *Synaptic mechanisms underlying the intense firing of neocortical layer 5B pyramidal neurons in response to cortico-cortical inputs.* Brain Struct Funct, 2019. **224**(4): p. 1403-1416.
79. Rolls, E.T. and W.P.C. Mills, *Computations in the deep vs superficial layers of the cerebral cortex.* Neurobiol Learn Mem, 2017. **145**: p. 205-221.
80. Heine, L., et al., *Resting state networks and consciousness: alterations of multiple resting state network connectivity in physiological, pharmacological, and pathological consciousness States.* Front Psychol, 2012. **3**: p. 295.
81. Jurkiewicz, M.T., A.P. Crawley, and D.J. Mikulis, *Is Rest Really Rest? Resting-State Functional Connectivity During Rest and Motor Task Paradigms.* Brain Connect, 2018. **8**(5): p. 268-275.
82. Hooks, B.M., et al., *Organization of cortical and thalamic input to pyramidal neurons in mouse motor cortex.* J Neurosci, 2013. **33**(2): p. 748-60.
83. Mao, T., et al., *Long-range neuronal circuits underlying the interaction between sensory and motor cortex.* Neuron, 2011. **72**(1): p. 111-23.
84. Bause, J., et al., *Impact of prospective motion correction, distortion correction methods and large vein bias on the spatial accuracy of cortical laminar fMRI at 9.4 Tesla.* Neuroimage, 2019. **208**: p. 116434.
85. Viessmann, O., et al., *Dependence of resting-state fMRI fluctuation amplitudes on cerebral cortical orientation relative to the direction of B0 and anatomical axes.* Neuroimage, 2019. **196**: p. 337-350.
86. Baez-Yanez, M.G., et al., *The impact of vessel size, orientation and intravascular contribution on the neurovascular fingerprint of BOLD bSSFP fMRI.* Neuroimage, 2017. **163**: p. 13-23.
87. Uludag, K. and P. Blinder, *Linking brain vascular physiology to hemodynamic response in ultra-high field MRI.* Neuroimage, 2018. **168**: p. 279-295.
88. Havlicek, M. and K. Uludag, *A dynamical model of the laminar BOLD response.* Neuroimage, 2020. **204**: p. 116209.
89. Marquardt, I., et al., *Cortical depth profiles of luminance contrast responses in human V1 and V2 using 7 T fMRI.* Hum Brain Mapp, 2018. **39**(7): p. 2812-2827.
90. Schweisfurth, M.A., et al., *Comparison of fMRI Digit Representations of the Dominant and Non-dominant Hand in the Human Primary Somatosensory Cortex.* Front Hum Neurosci, 2018. **12**: p. 492.
91. Glover, G.H., T.Q. Li, and D. Ress, *Image-based method for retrospective correction of physiological motion effects in fMRI: RETROICOR.* Magn Reson Med, 2000. **44**(1): p. 162-7.